# Welding Parameter Dependent Microstructure and Mechanical Properties of Friction Stir Welded High Carbon Steel Plates†

**SUN Yufeng*, FUJII Hidetoshi****

**Abstract**

*SK4 high carbon steel plates (0.95% C) with a thickness of 2 mm were subjected to the friction stir welding (FSW) process. After welding, three different types of microstructures were obtained in the stir zone depending on the different welding conditions. When FSW was carried out at 120 rpm, a refined ferrite matrix distributed with small cementite particles was formed in the entire stir zone. At 200 rpm, a refined pearlite phase was formed in the stir zone, together with a small amount of the martensite phase. However, at 400 rpm, a twin martensite structure became the dominate phase in the stir zone, accompanied by a small amount of the pearlite phase. The tensile tests revealed that the tensile strengths of the weld metals were higher than that of the base metal and increased with the increasing rotation speed. However, the elongations decreased. This study showed that the properties of the friction stir welded high carbon steel can be easily controlled by simply changing the welding conditions.*

**KEY WORDS: (Friction stir welding) (Microstructure) (Mechanical property) (high carbon steel)**

## 1. Introduction

Friction Stir Welding (FSW) is a relatively new solid-state joining technique, which was invented by the Welding Institute (TWI) of the UK in 1991 with the original purpose of joining Al and Al alloys, because Al alloys are very difficult to weld by conventional fusion welding methods [1]. During FSW a rotating tool is plunged into the work-piece and traverses along the weld path, by which the surrounding material around the rotating tool can be plastically deformed (stirred) and transported from the front to the back of the tool. Therefore, the work-pieces can be stirred together to form a joint [2-3]. Since the emergence of FSW, it has attracted great attention due to the advantages over conventional fusion techniques, such as higher joint efficiency, less distortion, lower residual stress and lower investment. The FSW technique has been mainly applied to the welding of light materials like Al and Mg alloys [4-6]. Recently, with the improvement of the FSW technique and the rapid development of highly durable rotating tools, this technique has been expanded to many high melting points materials including Cu, Ti, Fe and steels [7-9]. Over these years, the FSW technique has been successfully used for the welding of high carbon steels [10-11], which are considered as unweldable materials by fusion welding methods due to the formation of the brittle martensitic phase. In addition, the microstructure of the stir zone can be easily controlled by simply adjusting the welding parameters like the rotation speed, welding speed or the applied load. For example, Chung et al. [12] successfully carried out the FSW of SK5 steel at a welding temperature below and above the A1 point, which has a carbon content of about 0.85%. The variations in the microstructural evolution and mechanical properties were investigated by changing the traveling speed but with a fixed rotation speed. Khodir et al. [13] also applied the FSW to the SK4 steel plates under varied rotation speeds, which has a carbon content of about 0.95%. As a result, a very complicated microstructure including duplex microstructure, martensite with retained austenite etc. can be obtained in the stir zone. Based on the above description, it was found that due to the complex material flow in the stir zone and the thermal-mechanical process imposed on the work-pieces, a very complicated and versatile microstructure can be formed in the welds of high carbon steel plates and significantly depends on the welding conditions and the properties of the material itself. However, the distribution of the resultant microstructure in the welds has not been fully characterized yet.

† Received on June 30th, 2014
* Specially Appointed Associate Professor
** Professor
Transactions of JWRI is published by Joining and Welding Research Institute, Osaka University, Ibaraki, Osaka 567-0047, Japan

**Table 1**. Chemical composition of the as-received SK4 steel plate

| Steel type | Chemical composition (mass%) | | | | | | | | | |
|---|---|---|---|---|---|---|---|---|---|---|
| | C | Si | Mn | P | S | Cr | Ni | Cu | Al | Fe |
| SK4 | 0.95 | 0.2 | 0.42 | 0.017 | 0.003 | 0.147 | 0.01 | 0.01 | 0.001 | Bal. |

In this study, FSW was applied to the welding of 2 mm thick SK4 high carbon steel plates under a stir-in-plate mode. Various rotation speeds over a wide range were tried in order to obtain different microstructure in the welds. After welding, the relationship between the microstructural evolution and mechanical properties of the FSW processed specimen were investigated and discussed.

## 2. Experimental

In this study, the as-received 2-mm thick SK4 high carbon steel plates were subjected to the FSW process using a load-controlled FSW machine and stir-in-plate welding was performed. The chemical composition of the steel plate is listed in Table 1. The rotating tool used for the welding was made of a WC-based material, which had a shoulder diameter of 12mm, probe diameter of 4mm and probe length of 1.8 mm. The tool axis was tilted by 3° with respect to the normal direction of the sample surface. The applied load was varied from 1.7 t to 2.5 t. The travelling speed of the rotating tool was kept constant at 100 mm/min and three rotation speeds of 120, 200 and 400 rpm were separately applied. Argon shielding gas was used during the welding process to protect the plate surface from oxidation. Three types of microstructures were thus produced in the stir zone, which are dependent on the various welding conditions used during the welding process.

The microstructures of the base metal and the welds produced at different rotation speeds were observed by optical microscope (OM), scanning electron microscope (SEM) and transmission electron microscope (SEM). For the OM and SEM observation, the samples were mechanically polished followed by chemical etching using 3% Nital solution. For the TEM observation, the samples were prepared by twin-jet electro-polishing with a solution of $HClO_4$:$CH_3COOH$=1:9. Because the stir zones of the joints show higher strength than that of the base metal, miniature tensile specimens were cut in a dog-bone shape with the gauge length of 6 mm, width of 3 mm and thickness of 2 mm. The tensile tests for the specimens were carried out using an Instron tensile machine at a cross-head speed of 0.5 mm/min. After the tensile tests, the morphology of the fractured plane was characterized by SEM.

## 3. Results and Discussion

**Fig. 1(a)-(c)** show the typical appearances of the friction stir welds produced at the rotation speeds of 120, 200 and 400 rpm, respectively. Generally speaking, the amount of flash along the weld seam increased with the increasing rotation speed, and showed the same trend as the other friction stir welded materials. Especially, for the one welded at 400 rpm, superfluous flash was generated due to the too high heat input. This result shows that the FSW of high carbon steel plates can be performed within a very wide range of welding conditions, although they are generally regarded as un-weldable materials by fusion welding methods. In addition, the heat input generated by friction between the tool and the work-piece has a linear relationship with the rotation speed, travel speed and the applied load [14]. Therefore, the friction heat generated during the FSW at 400 rpm is estimated to be more than 2 times higher than that generated at 120 rpm. The higher heat input will inevitably result in a higher welding temperature, which will finally cause a different microstructure in the welds after cooling from the welding temperature.

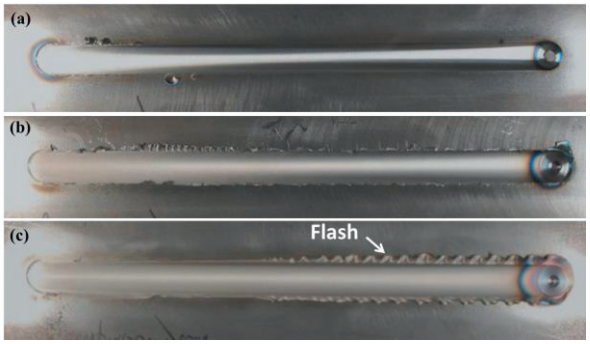


**Fig. 1** The typical appearance of the friction stir welds obtained the rotation speed of (a) 120 rpm; (b) 200 rpm; and (c) 400 rpm

After welding, the cross-sectional macrostructures of the welds produced at the different rotation speeds are shown in **Fig. 2**. No welding defects were observed in any of the joints. In the friction stir welded materials, several specific zones are generally classified, namely, the stir zone, thermo-mechanically affected zone (TMAZ), heat affected zone (HAZ) and the base metal. As shown in **Fig. 2**, the area size of both the stir zone and the TMAZ increased with the increasing rotation speed, or with the heat input. Due to the inhomogeneous materials flow in the welds, the TMAZ has a larger area on the retreating side (RS) than on the advancing side (AS). However, the HAZ is difficult to be distinguished in this study. In addition, the different contrast in the stir zone indicates that the microstructure in the stir zone varied with the different rotation speeds. In the sample welded at 120 rpm as shown in **Fig. 2(a)**, the stir zone contains a refined microstructure compared with that of the base metal.

There is a clear boundary between the stir zone and the base metal. For the sample welded at 200 rpm as shown in **Fig. 2(b)**, a lot of small white phases can be found distributed in the top region of the stir zone. The white phase was confirmed to be martensite phase, formed due to the higher temperature in the top region of the stir zone during the welding process. As for the joint welded at 400 rpm shown in **Fig. 2(c)**, the stir zone was mainly composed of the martensite phase. In addition, the martensite region was prone to be formed in the stir zone near the advancing side, which reveals that the advancing side has a slightly higher temperature than the retreating side.

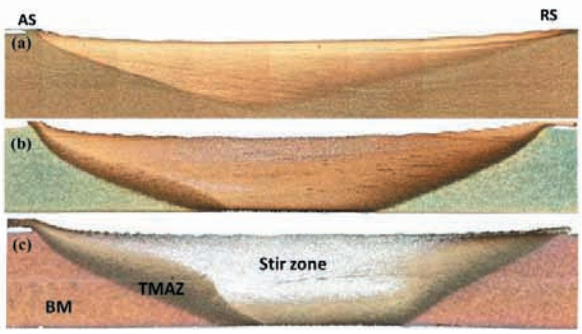


**Fig. 2** Cross-sectional macrostructures of the welds obtained at the rotation speeds of (a) 120 rpm; (b) 200 rpm and (c) 400 rpm

**Fig. 3** shows the higher magnification OM images of the TMAZ in the welds obtained at different rotation speeds. It is said that to clarify the microstructural evolution in the TMAZ is of great significance, although the TMAZ is generally very small and maybe negligible. On the other hand, it is very essential to understand how the original microstructure in the BM evolves into that in the SZ due to the transitional nature of the TMAZ. In addition, the TMAZ may be the weakest region and thus become the failure position during the tensile tests [15]. According to **Fig. 3(a)**, the TMAZ in the 120 rpm welds is very narrow, and consists of elongated ferrite grains and refined cementite particles. When the rotation speed increased to 200 rpm and 400 rpm, it was found that the TMAZ in the welds became wider and contained a transient microstructure within the TMAZ bands. The TMAZ can be simply divided into two regions, namely, TMAZ-1 and TMAZ-2, as indicated in **Fig. 3(b) and (c).** TMAZ-1 is close to the base metal and mainly consists of a refined but deformed ferrite matrix and smaller cementite particles, which is similar to the microstructure of the TMAZ in **Fig. 3(a).** The small cementite particles were distributed along the border of the SZ, namely, the shear direction. However, the TMAZ-2 is close to the stir zone and mainly consists of refined pearlite structure and distributed cementite particles. In addition, the cementite particles also were distributed parallel to the shear direction, which indicated the deformation characteristic, a typical feature of the TMAZ. One of the enlarged microstructures in the area between TMAZ1 and TMAZ 2 was observed by SEM and shown in **Fig. 4**. Therefore, the boundary between TMAZ1 and TMAZ2 can also be regarded as the division line of the welding temperature, namely; the welding temperature is higher than the Ac1 point on the right side of the boundary. However, the welding temperature is lower than the Ac1 point on the left side of the boundary.

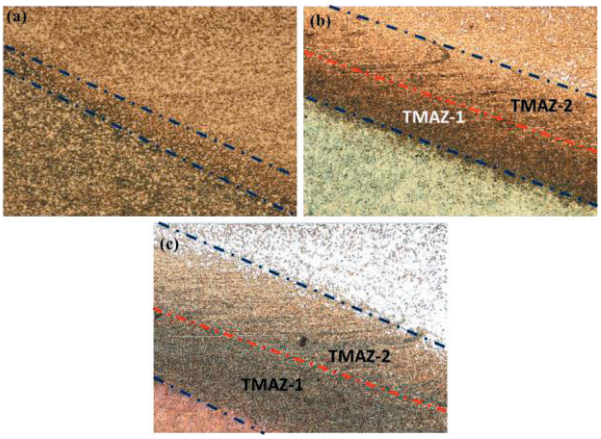


**Fig. 3** The enlarged OM images of the TMAZ in the welds obtained at a rotation speed of (a) 120 rpm; (b) 200 rpm and (c) 400 rpm

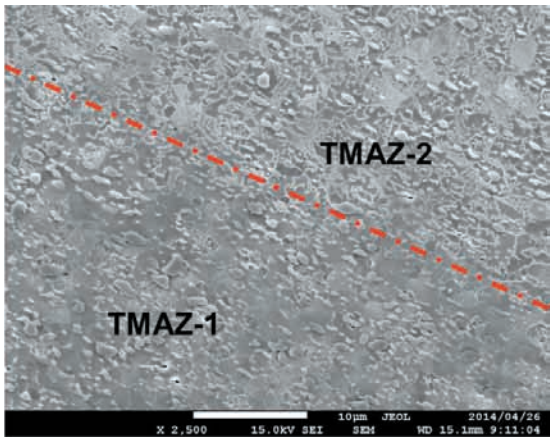


**Fig. 4** SEM image showing the boundary between TMAZ-1 and TMAZ-2

**Fig. 5** shows the microstructure of the stir zone welded at different rotation speeds, together with that of the base metal for comparison. The microstructure of the base metal shown in **Fig. 5 (a)** consists of a pearlite structure and cementite particles, which have an average size of about 10 μm and 3 μm, respectively. **Fig. 5(b)** shows the microstructure of the stir zone welded at 120 rpm, which consisted of a remarkably refined ferrite matrix distributed with a high density of cementite particles. The ferrite matrix has an average grain size of about 3 μm. However, the cementite particles consist of two types of particles, one is a short-rod like particle which is supposed to be formed from the breaking of the cementite lamellar in the pearlite structure of the base metal during the welding process. The other type of cementite particle is slightly larger and has an irregular shape, which is

supposed to come from particles originally distributed in the base metal. It was revealed that the welding process at 120 rpm was carried out below the Ac1 phase transformation point. **Fig. 5(c)** shows the microstructure of the stir zone welded at 200 rpm, which consisted of a pearlite phase and a small amount of the martensite phase. It was revealed that the welding temperature is above the Ac1 point and phase transformation took place after the welding process. **Fig. 5(d)** shows the microstructure of the stir zone welded at 400 rpm, which mainly consisted of the martensite phase and a small amount of the pearlite phase, as indicated by the arrow in the figure.

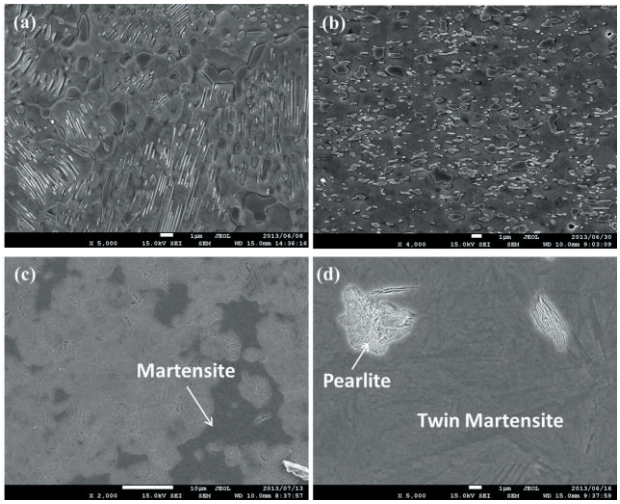


**Fig. 5** SEM images showing the microstructure in the (a) base metal; and the stir zone welded at (b) 120 rpm; (c) 200rpm and (d) 400 rpm

To further clarify the microstructure in the stir zone, TEM observation of the stir zone were carried out for all the welds obtained under the different welding conditions. **Fig. 6** shows the corresponding TEM images and that of the base metal was also included for comparison. In the base metal as shown in **Fig. 6(a)**, the typical microstructure of the hyper-eutectoid Fe-C binary alloy can be observed. The long rod-like cementite phases were distributed parallel to each other in the ferrite matrix. In addition, some block cementite particles with irregular shapes were embedded either on the ferrite grain boundary or inside the grains. In the stir zone welded at 120 rpm as shown in **Fig. 6(b)**, a microstructure of ferrite matrix distributed with a highly density of small cementite particles could be distinguished. However, the long rod-like cementite phases cannot be found any more, and are supposed to be fractured into small particles by the severe stirring of the rotating tool during the welding process. In addition, high dense dislocations could be observed in the ferrite matrix, but with tangling along the cementite particles as indicated in the figure. **Fig. 6(c)** shows the microstructure of the stir zone welded at 200 rpm, in which a typical pearlite structure containing an alternating lamellar cementite phase and ferrite phase was observed. Some block cementite particles can also be found distributed along the boundary of the pearlite colony. Compared with the base metal, the pearlite colony size is quite small in the stir zone after the FSW. In addition, the lamellar width of the cementite phase is also smaller than that in the base metal. **Fig. 6(d)** shows the microstructure of the stir zone welded at 400 rpm, which shows a typical martensite structure containing a high density of twin lamellar. The twin lamellar width is several tens of nanometers.

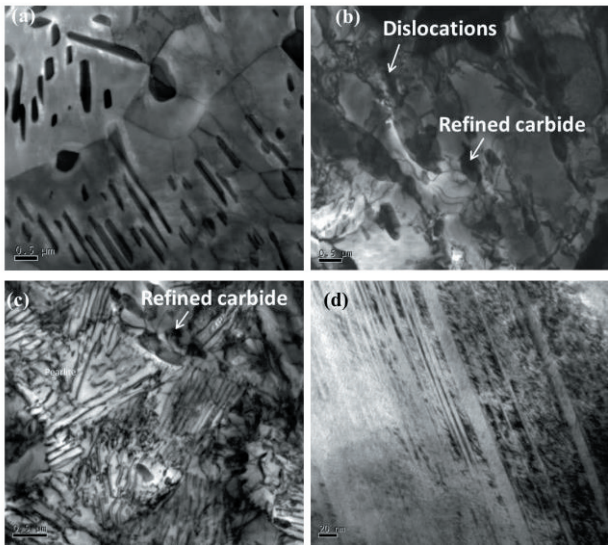


**Fig. 6** TEM images showing the microstructure of the (a) base metal; and the stir zone welded at (b) 120 rpm; (c) 200rpm and (d) 400 rpm

After welding, two lines of hardness tests were carried out along the cross-sectional plane of the welds obtained at different rotation speeds. **Fig. 7** shows the profile of the hardness distribution in the stir zone and the position for the hardness measurement was also indicated in the photo inserted in the figure. Generally, the hardness in the stir zone is higher than that of the base metal and increases with the increasing rotation speed. In addition, the distribution of the hardness increment in the top region of the stir zone is wider than that in the bottom region, due to the basin-like stir zone caused by the material flow during the welding process. After welding at 120 rpm, the top region and bottom region in the stir zone show a hardness of about 400 HV and 300 HV, respectively. Both are higher than the 230 HV of the base metal. After welding at 200 rpm, the top region in the stir zone shows a constant hardness value of about 800 HV. However, the bottom region shows a maximum hardness value of about 800 HV, but with a valley on the profile of the hardness distribution. The hardness drop at the center of the bottom region in the stir zone may be caused by the slow cooling rate therein after the welding process, which consequently results in the formation of the coarse pearlite structure. After welding at 400 rpm, both the top and bottom region in the stir zone show a constant hardness value, which is as high as about 880 HV due to the formation of the hard martensite phase.

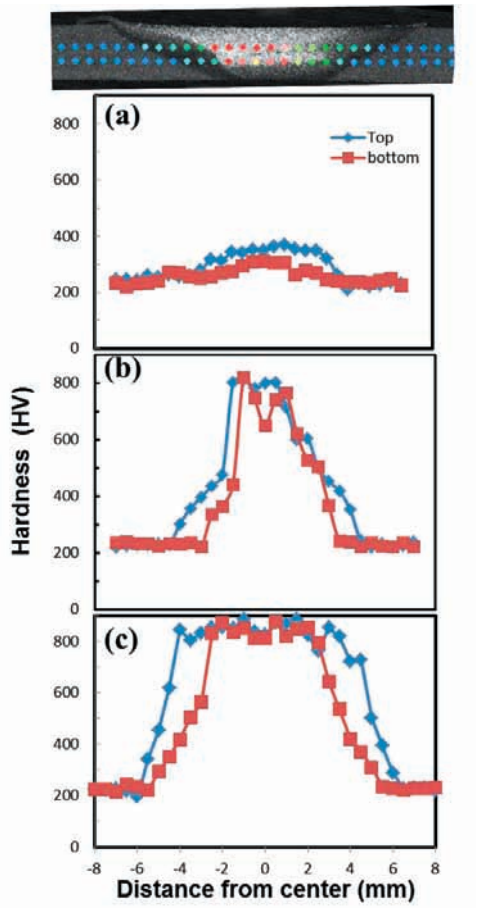


**Fig. 7** The hardness distribution along the cross-sectional plane in the joints welded at (a) 120 rpm; (b) 200 rpm and (c) 400 rpm.

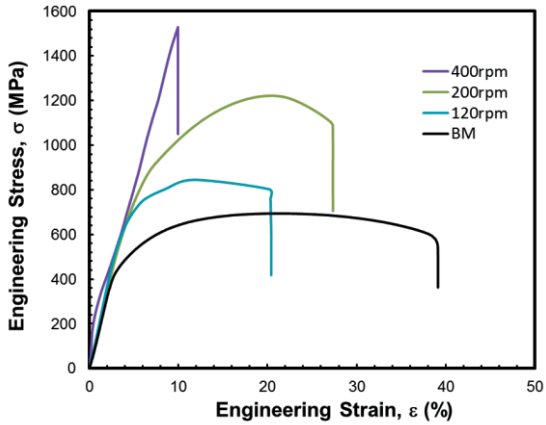


**Fig. 8** The tensile strain-stress curves of the base metal and the joints welded at different rotation speed

The specimens produced at the different rotation speeds were subjected to tensile tests, together with the base metal. The tensile strain-stress curves are shown in **Fig. 8** and **Table 2** summarizes the yielding strength, ultimate tensile strength and elongation of the specimens welded at the different rotation speeds, together with that of the base metal. For all the specimens obtained under the different welding conditions, the yielding point and the fracture strength are higher than that of the base metal, however, with reduced elongation. Especially for the welds prepared at a rotation speed of 400 rpm, the tensile specimen show the very high fracture strength of 1520 MPa due to the formation of the hard twin martensite phase. However, the specimen shows a nearly zero elongation because of the intrinsic brittleness of the martensite phase containing a high carbon content.

**Table 2**. Summary of the mechanical properties of the joints welded at different rotation speed

| | $\sigma_{ys}$ (MPa) | $\sigma_{uts}$ (MPa) | ε (%) |
|---|---|---|---|
| BM | 420 | 695 | 36 |
| 120 rpm | 650 | 840 | 17 |
| 200 rpm | 850 | 1250 | 22 |
| 400 rpm | 1520 | 1520 | 0 |

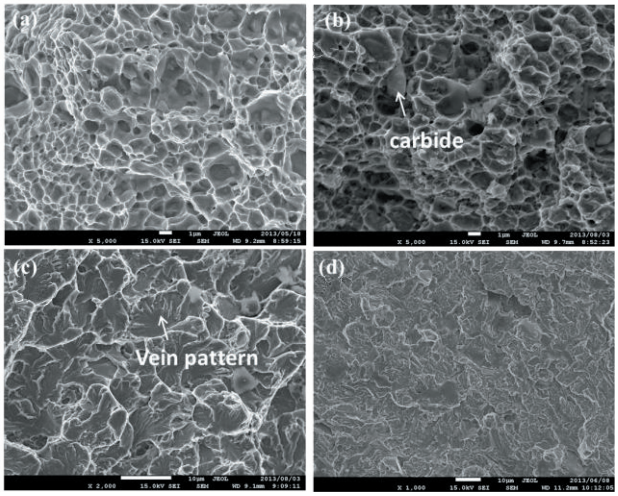


**Fig. 9** SEM images showing the morphology of the fractured plane of the (a) base metal; and the friction stir welded steel plates obtained at the rotation speeds of (b) 120 rpm; (c) 200 rpm and (d) 400 rpm.

**Fig. 9** shows SEM images comparing the morphology of the fractured plane of the tensile specimens. **Fig. 9** (a) shows the fractured plane of the BM, which revealed a ductile fracture surface containing considerable dimples resulting from a microvoid coalescence (MVC). The fractures surfaces of the specimen welded at 120 rpm are shown in **Fig. 9 (b),** which were characterized by a very fine dimple pattern resulting from the MVC. However, the carbide particles can be observed to be embedded in the dimple on the fractured surface of the specimen, which indicated the strong interfacial bonding between the cementite particles and ferrite matrix. **Fig. 9 (c)** shows the morphology on the fractured plane of the specimen welded at 200 rpm, which shows a clear vein-pattern

morphology on the fractured surface. The vein-like feature may be caused by the transverse fracture of the lamellar ferrite/cementite structure in the pearlite packet. **Fig. 9 (d)** shows the morphology of the fractured plane welded at 400 rpm, which shows a small smooth plane indicating the brittleness of the materials.

## 4. Conclusions

The results of this study reveal that a high carbon steel alloy can be successfully welded by the FSW technique within a wide welding range. According to the investigation of the microstructure and mechanical properties determined by the relevant welding conditions, the following conclusions could be drawn.

a) The high carbon steel alloy can be successfully friction stir welded at different rotation speeds, which result in different microstructures and mechanical properties in the welds.
b) When the FSW is performed at 120 rpm, the welding temperature is below the Ac1 point and a homogeneous microstructure of cementite distributed in the ferrite matrix is formed. When performed at 200 rpm, the weld has a microstructure of pearlite and a small amount of the martensite phase. When performed at 400 rpm, the weld has a microstructure of the twin martensite phase and a small amount of the pearlite phase.
c) Compared with the base metal, the welds prepared at the different rotation speeds show a higher tensile strength, however, with reduced elongation.

## Acknowledgement

The authors wish to acknowledge the financial support of the Japan Science and Technology Agency (JST) under Collaborative Research Based on Industrial Demand "Heterogeneous Structure Control: Towards Innovative Development of Metallic Structural Materials", a Grant-in-Aid for the Cooperative Research Project of National Wide Joint-Use Research Institute, the Global COE Programs from the Ministry of Education, Sports, Culture, Science, and a Grant-in-Aid for Science Research from the Japan Society for Promotion of Science and Technology of Japan, and ISIJ Research Promotion Grant.

## References

[1] Thomas WM, Nicholas ED, Needham JC. International Patent Application No. PCT/GB92/02203 (1991).
[2] Mishra RS, Ma ZY. *Mater. Sci. Eng, R* 2005; 50: 1-78
[3] Nandan R, Debroy T, Bhadeshia HKDH. *Prog. Mater. Sci*, 2008, 53: 980-1023
[4] Sun YF, Fujii H, Takada Y, Tsuji N, Nakata K, Nogi K. Mater. Sci. Eng. A, 2009, 527, 317-321.
[5] Chen J, Fujii H, Sun YF, Morisada Y, Kondoh K. Mater. Sci. Eng A, 2012, 549, 176-184
[6] Ma ZY, Pilchak AL, Juhas MC and Williams JC. Scripta Mater, 2008, 58, 361.
[7] Sun YF, Fujii H. Mater. Sci. Eng, A. 2010, 527: 6879-6886.
[8] Fujii H, Sun YF, Kato H. Mater. Sci. Eng. A, 2010, 527: 3386-3391.
[9] Sato YS, A Shiota, Kokawa H. Sci. Tech. Weld. Join., 2009, 14: 202-209.
[10] Fujii H, Cui L, N Tsuji, Maeda M, Nakata K and Nogi K. Mater. Sci. Eng. A, 2006, 429: 50-57.
[11] Cui L, Fujii H, Tsuji N and Nogi K.. Scripta Mater., 2007, 56: 637-640.
[12] Chung YD, Fujii H, Ueji R, Tsuji N.. Scripta Mater., 2010, 63: 223-226.
[13] Khodir SA, Y Morisada, R Ueji, H Fujii. Mater. Sci. Eng A, 2012, 558, 572-578.
[14] Frigaard O, Grong O and Midling OT. Metall. Mater. Trans. A, 2001, 32, 1189-1200.
[15] Wu LH, Wang D, Xiao BL and Ma ZY. Scripta Mater, 2014, 78-79, 17-20.